EFFECTS OF DIFFERENT OIL RETURN PIPE LOCATIONS ON THE VORTEX CHARACTERISTICS OF A CYLINDRICAL CYCLONE SEPARATOR

Zeming FU [1], Huagen WU [1]*, Mengtao LIANG [1], Zhendong GUO [1], Guanghua WU [1], Shuo SHANG [2], Liang HOU [1] and Xin ZHANG [3]

[1] School of Energy and Power Engineering, Xi'an Jiaotong University, Xi'an, China

[2] School of Water and Environment, Chang'an University, Xi'an, China

[3] School of Resources Engineering, Xi'an University of Architecture and Technology, Xi'an, China

* Corresponding author, E-mail: hgwu@mail.xjtu.edu.cn

The optimization of internal components in the oil-gas separator is crucial for enhancing the performance of the compressor system. In this reported study, the effects of three different oil return pipe locations on the vortex characteristics of a cylindrical cyclone separator are investigated by CFD simulation based on the omega method, and the relationship with the separation performance is analyzed. The vortex deformation and breakup near the oil return pipe are evident, with the degree following the order of C > B > A, which is conducive to reducing pressure loss. Cyclone C, with the inclined return pipe, exhibits the lowest pressure drop. The overall separation efficiency follows the sequence of A > B > C. For oil droplets of 5μm and larger, the separation efficiency is essentially the same, exceeding 97.5 %. Cyclone A exhibits the best separation effect for oil droplets smaller than 5μm. This study provides some references for optimizing the internals of oil separators.

Keywords: *Cyclone separator; vortex structure; oil return pipe; oil-gas separation*

1. Introduction

For oil-injected screw compressor system, the installation of an efficient oil-gas separator at the discharge outlet not only ensures the purity of the discharge gas and system efficiency [1, 2], but also improves the recyclability of the lubricating oil [3]. The oil-gas cyclone separator is widely employed in the chemical industry fields because of its simple design, small size and good separation effect [4, 5], and is also the most commonly used primary separator of oil and gas in oil-injected compressor systems [6]. The centrifugal force and differential density between the droplets and the working fluid are used to separate the droplets. The oil-gas mixture flows into the cyclone from the inlet pipe in the direction of tangency, and oil droplets tend to move in the radial outer direction because of the greater centrifugal force. When oil droplets hit the inner wall of the cylindrical cyclone, they adhere to the wall and flow downward, and are discharged from the oil return pipe after reaching the bottom. The gas flows out of the exhaust pipe to achieve oil-gas separation [7].

Many scholars have conducted researches to optimize the structure to improve separation performance, including vortex finder insertion depth and diameter, cyclone length, the number of inlets

and inlet size [8, 9]. In addition, effective internal component design is crucial for improving separation performance, as it directly influences the flow field characteristics within a cyclone separator. According to Wakizono et al. [10], a conical ring mounted on the top portion of the vortex detector allows for a lowest cut size of 50 % and the highest overall separation efficiency of particles. Some studies have shown that the installation of an extra rod-like member inside a cyclone can have a positive impact. Gong et al. [11] added the Repds to the cyclone and found a significant reduction in pressure drop. Liu et al. [12] analyzed the drag reduction mechanism of Repds using Laser Doppler Velocimetry (LDV), and the findings revealed that the installation of Repds could significantly weaken the turbulent dissipation, lower the tangential velocity and velocity gradient, and lessen the pressure loss. Brunmair et al. [13] installed the pipe along the entire length of the cyclone's central axis and then found that this improved solution resulted in more stable internal vortex and prevented the processing of vortex core (PVC) phenomenon. Pan et al. [14] determined that adding the helical guide vanes to the cyclone helped to increase the spiral motion of the airflow and greatly enhanced the separation efficiency. Zhou et al. [15] further explored the effect of spiral guide vane rotation number on the flow field distribution, turbulence intensity and separation performance of Stairmand cyclone by experimental tests and numerical approaches. Chen et al. [16] developed a combined central column and helical guide vanes inner member and performed numerical simulations and experimental tests to investigate the influence of this inner member on the separation effect and flow field characteristics of a divergent cyclone. The oil return pipe, functioning as an internal component, is a common feature in oil-gas cyclone separators within compressor systems. In contrast, cyclone separators used in other industrial applications, such as gas-solid separation, do not include this internal structure. Consequently, there has been relatively limited research in the published literature regarding the optimization of oil return pipes.

This study employs numerical method to investigate how three different positions of the return oil pipe affect the vortex characteristics of a cylindrical cyclone separator and their relationship with separation performance. The novelty of this research lies in its use of the omega method to discern variations in vortex distribution, enabling a discussion on optimal return oil pipe arrangements. This approach maximizes system performance and efficiency, providing valuable insights for practical engineering applications.

2. Numerical simulation

2.1. CFD model

The gas Mach number in a cyclone is usually less than 0.3 and is assumed to be an incompressible flow. The continuity and Reynolds-averaged Navier-Stokes (RANS) equations can be written as [17]:

$$\frac{\partial \overline{u_i}}{\partial x_i} = 0 \tag{1}$$

$$\frac{\partial \overline{u_i}}{\partial t} + \overline{u_j}\frac{\partial \overline{u_i}}{\partial x_j} = -\frac{1}{\rho}\frac{\partial \overline{P}}{\partial x_i} + \nu\frac{\partial^2 \overline{u_i}}{\partial x_j\,\partial x_j} - \frac{\partial}{\partial x_j}R_{ij} \tag{2}$$

Here, u_i represents gas velocity, x_i, x_j, x_k denote the direction in the coordinate system. ρ and ν are the gas density and kinematic viscosity, while P is the pressure. Additionally, $R_{ij} = \overline{u_i' u_j'}$ is the Reynolds stresses, u' is the fluctuation of velocity.

The whirling gas flow in a cyclone is a very sophisticated turbulent flow. In past studies, the RSM turbulence model has been extensively utilized and verified in CFD simulation research of cyclone separators due to its high accuracy in predicting cyclonic flow [18, 19]. The transmission equation in the RSM can be written as:

$$\frac{\partial}{\partial t}R_{ij}+\overline{u_k}\frac{\partial}{\partial x_k}R_{ij}=\frac{\partial}{\partial x_k}\left(\frac{\nu_t}{\sigma^k}\frac{\partial}{\partial x_k}R_{ij}\right)-\left[R_{ik}\frac{\partial\overline{u_j}}{\partial x_k}+R_{jk}\frac{\partial\overline{u_i}}{\partial x_k}\right]-\mathrm{C}_1\frac{\varepsilon}{k}\left[R_{ij}-\frac{2}{3}\sigma_{ij}K\right]-C_2\left[P_{ij}-\frac{2}{3}\sigma_{ij}P\right]-\frac{2}{3}\sigma_{ij}\varepsilon \tag{3}$$

The term turbulence production term P_{ij} is defined as follows:

$$P_{ij}=-\left[R_{ik}\frac{\partial\overline{u_j}}{\partial x_k}+R_{jk}\frac{\partial\overline{u_i}}{\partial x_k}\right],P=\frac{1}{2}P_{ij} \tag{4}$$

P represents the fluctuating kinetic energy production, ν_t stands for eddy kinematic viscosity, $\sigma^k=1$, $\mathrm{C}_1=1.8$, $\mathrm{C}_2=0.6$ is an empirical constant. The transport equation for turbulent dissipation rate ε is as follows:

$$\frac{\partial\varepsilon}{\partial t}+\overline{u_j}\frac{\partial\varepsilon}{\partial x_j}=\frac{\partial}{\partial x_j}\left[\left(\nu+\frac{\nu_t}{\sigma^\varepsilon}\right)\frac{\partial\varepsilon}{\partial x_j}\right]-C^{\varepsilon1}\frac{\varepsilon}{K}R_{ij}\frac{\partial\overline{u_i}}{\partial x_j}-C^{\varepsilon2}\frac{\varepsilon^2}{K} \tag{5}$$

where $K=\frac{1}{2}\overline{u_i'u_j'}$ is the fluctuating kinetic energy. The constant values are $\sigma^\varepsilon=1.3$, $C^{\varepsilon1}=1.44$, $C^{\varepsilon2}=1.92$

Due to the low oil droplet content, usually less than 5 % volume fraction, the interplay of oil droplets with the air and the interaction between oil droplets can be ignored [20]. A one-way coupled Euler-Lagrange method was used in the simulation. The force balance equation according to the Newton's second law can be expressed as:

$$\frac{du_{pi}}{dt}=F_D(u_i-u_{di})+\frac{g(\rho_d-\rho)}{\rho_d} \tag{6}$$

Where: $\vec{u}_d$ denotes the droplet velocity, ρ_d represents the droplet density and F_D denotes the drag force of gas on the oil droplets, which is defined as:

$$F_D=\frac{18\mu}{\rho_d D_d^2}\cdot\frac{C_D\mathrm{Re}}{24} \tag{7}$$

$$C_D=a_1+\frac{a_2}{\mathrm{Re}}+\frac{a_3}{\mathrm{Re}^2} \tag{8}$$

Where D_d is the droplet diameter,C_D is the drag coefficient. a_1, a_2 and a_3 are constant that depends on the Reynolds number.

Additionally, the influence of turbulence on small oil droplets cannot be neglected. To enhance the accuracy of separation efficiency prediction, the discrete random walk (DRW) and the random eddy lifetime (REL) were applied to account for droplet turbulence dispersion [21, 22].

2.2. Computational geometry

This study compared the vortex characteristics and separation effect based on three cylindrical cyclone separators with different oil return pipe locations, as shown in fig. 1, corresponding to cyclone

A, B and C. The physical dimension was set according to the actual application of an oil separator. The units for geometric dimensions are in millimeters.

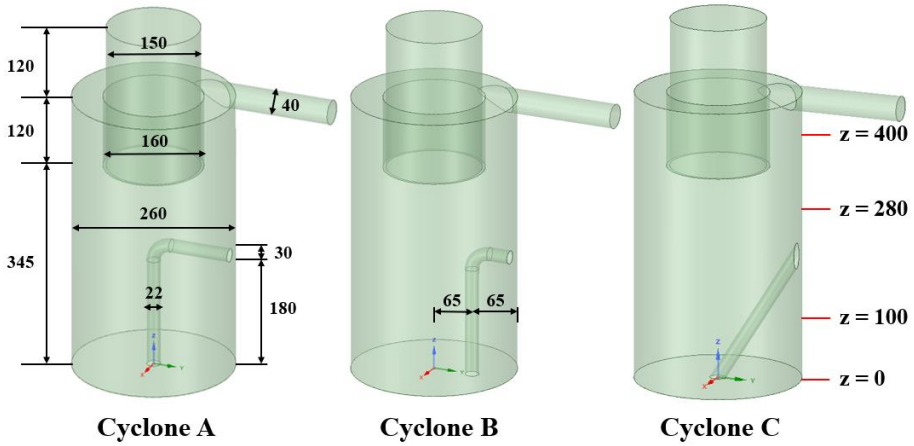

Figure. 1 Structure diagram of three oil return pipe arrangements.

2.3. Solver setting

This study conducted simulations of the flow field using the commercial CFD software ANSYS FLUENT based on the finite volume method. For coupling pressure and velocity, the SIMPLEC method was selected. The PRESTO! and QUICK schemes were used in the pressure interpolation and discretization of momentum. The second-order upwind scheme was applied for discretizing turbulent kinetic energy and turbulent dissipation rate, with a relaxation factor set to 0.8. The first-order upwind scheme was utilized for calculating Reynolds stress, with a relaxation factor set to 0.5. The transient solver was utilized with a time step of 0.0001 s and 30 iterations per step. The discrete phase model was employed to calculate the separation efficiency of oil droplets, with a maximum step number of 500,000 and a step length factor of 5. The convergence criteria were fixed at 10^{-5} for the scaled residual components.

2.4. Boundary conditions

The boundary condition for the cyclone entrance was specified as a velocity inlet, while the exhaust outlet was designated as a pressure outlet. The inlet gas velocity was set to 15 m/s, with dynamic viscosity and density were referred to Gao et al. [5]. A no-slip boundary condition was set and the treatment of the near wall was a standard wall function. The discrete oil droplets were considered as spherical particles with a density of 900 kg/m^3. For droplets larger than 10 μm, the cyclone separator demonstrates a collection efficiency exceeding 99 %. The experimental results indicated that there were nearly no oil droplets larger than 10 μm at the outlet [2]. Hence, the Rosin-Rammler function was used to depict the inlet distribution of oil droplets, as shown in fig. 2, which illustrates the cumulative distribution. The oil droplets range in size from 1 μm to 10 μm, with a mean diameter of 4.31 μm and a dispersion coefficient of 2.46. They were introduced at the inlet with the same initial velocity as the air. The boundary conditions on the bottom wall and the cylindrical body were configured as trap. Droplets passing through the cyclone separator and reaching the outlet surface were considered as escaping, whereas those colliding with the oil return pipe surface were considered to be reflected. The feasibility of the boundary condition settings has been verified in previous research [4, 23].

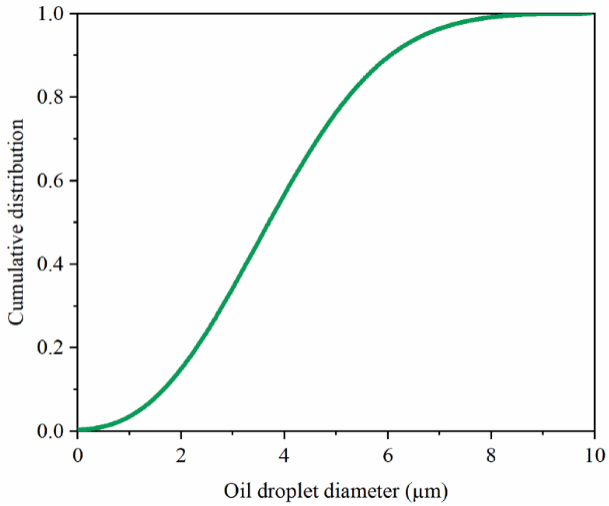

Figure. 2 Particle cumulative distribution function curve.

2.5. Grid independence

To ensure the independence of gird, three levels of grids of cyclone A were examined in our preliminary calculation containing 388245, 527957, and 754321 grids. Figure. 3 shows the tangential velocity curves for the three grid levels at z=280 mm, with an air velocity of 15 m/s. It can be observed that the average error in the tangential velocity distribution is less than 3 % for all three grid levels. To ensure the best simulation results, the grid level with the highest number of grids was selected.

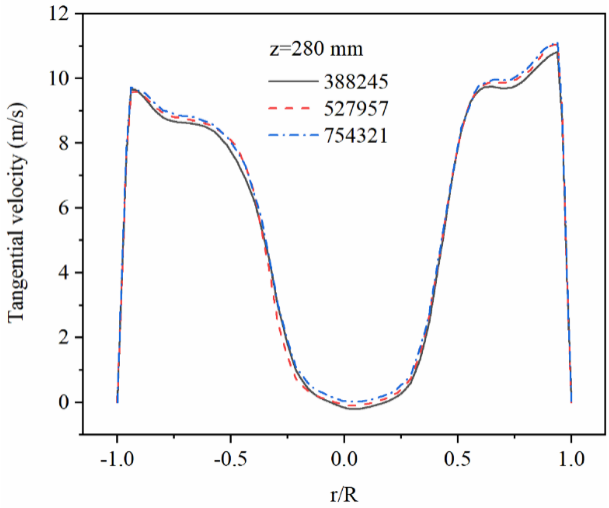

Figure. 3 Tangential velocity at z=280mm of the cyclone A of three grids.

3. Results and discussion

3.1. Model validation

To verify the numerical approach of this study, the experimental data [24, 25] were used for comparative analysis. The simulation here were performed with the precise geometry of the cyclone in their experiments. Figure 4 illustrates the comparison between simulation and experimental results. After calculations, the separation efficiency exhibits an average deviation of 1.16 %, while the average

deviation in pressure drop emerges as 8.56 % once the inlet velocity attains 15 m/s. The simulation of the tangential velocity distribution at the same location matches well with the experimental results. Overall, the simulated data are in good accord with the experimental test data and can faithfully reflect the flow and particle behavior of the flow field.

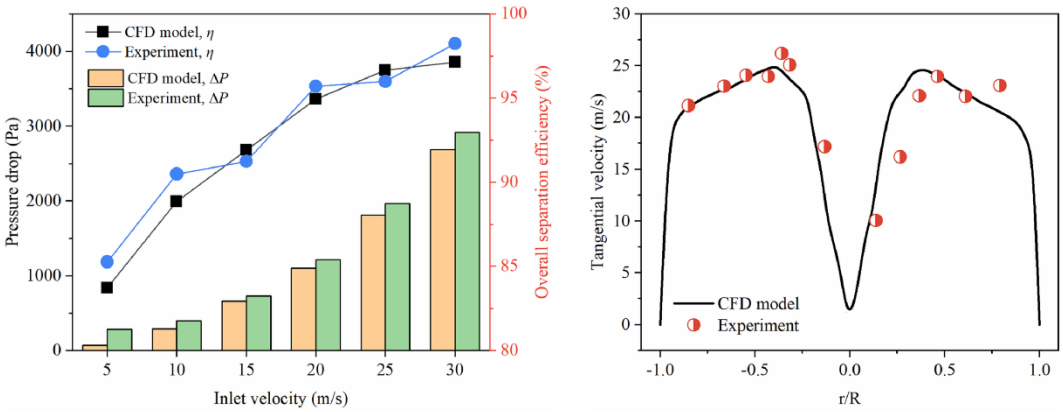

Figure. 4 Comparison of the simulation and experimental data.

3.2. The isovortex surface

The highly swirling fluid in a cyclone is a complex turbulent flow. For more accurate description of the vortex in cyclones, Li et al. [26] compared the vortex of cyclones identified by Q criterion and omega method. The results indicated that it was more accurate to obtain the vortex using the omega method, so the vortex of cyclones with three structures was analyzed based on the omega method. The detailed mathematical formulation of this method was given by Liu [27], and the area where $\Omega \geq 0.52$ represents the vortex .

The isovortex surface of the cyclone A, B and C is given in fig 5. For three different structures, the airflow in the entrance section is mainly laminar, almost no vortex is generated, so the energy loss is very little. The isovortex surface distribution in the cyclones is distorted rather than centered on the center axis. The equivalent diameter and deformation degree are two important aspects of evaluating the isovortex surface. The equivalent diameter is larger in the upper area of the cylinder and begins to decrease at about 1/2 the height of the cylinder, demonstrating that the kinetic energy contained in the vortex is gradually decreasing. The deformation degree is larger near the oil return pipe and the obvious vortex breaking can be seen, and the order of the degree of vortex distortion and breaking from high to low is C > B > A. Theoretically, the greater the degree of vortex distortion and breaking, the greater the kinetic energy dissipation, which can reduce the pressure loss [28, 29]. After calculation, the pressure drop of the cyclone A, B and C were 341.2 Pa, 303.4 Pa and 255.3 Pa respectively, which the order is consistent with the above law. Cyclone C, with a slanted oil return line, exhibits the lowest pressure drop. In comparison to cyclone A and B, cyclone C demonstrates a 25.18 % and 15.85 % reduction in pressure drop, respectively.

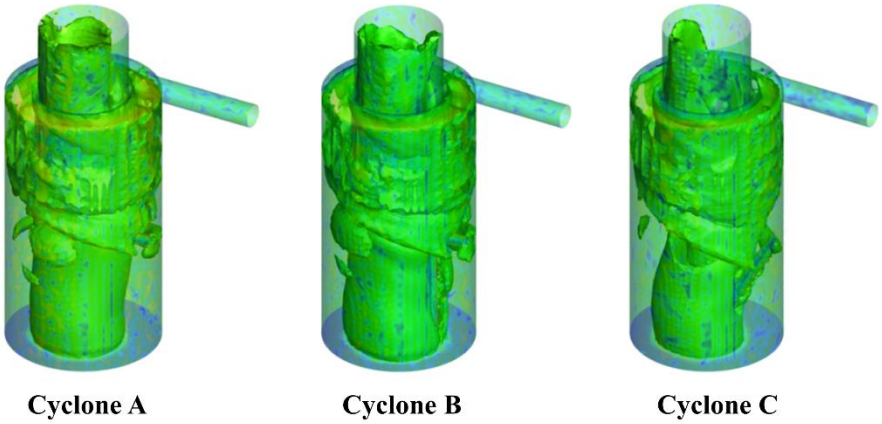

Figure. 5 The isovortex surface of cyclone A, B and C.

3.3. The vortex line diagram and vorticity magnitude

As shown in fig 6, the contours of vorticity magnitude were drawn on the cross-section to generate a vortex line diagram. The vortex lines are very complicated in the cyclone separator. The vortex lines are separated into inner and outer vortex streamlines, showing a stratified pattern. At z = 100 mm, compared to cyclones B and C, the vortex lines of cyclone A are more symmetrical and uniform, and the vortex center is closer to the center of geometry. This is due to the fact that the oil return pipe is installed at the bottom geometric center, where the vortex distribution is more uniform and regular, and the flow field is more stable and less turbulent. At z = 280 mm, for cyclones B and C, the departure of the central point of the vortex distribution from the geometric central axis is reduced. The distribution pattern of the vortex lines is more similar in three cyclones at z = 400 mm, indicating that the different location of the oil return pipe has a weak effect on the vortex in the upper part of the separator.

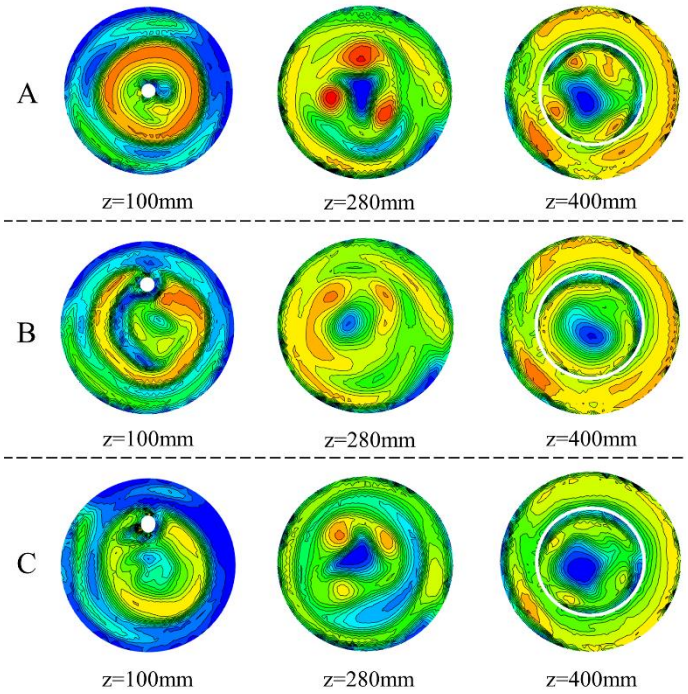

Figure. 6 The vortex line diagram of cyclone A, B and C.

Figure. 7 provides the vorticity magnitude distribution curves of three cyclones at z = 100 mm, 280 mm, and 400 mm. The vorticity curves of the three cyclones are asymmetric with respect to the radial position of the vorticity peaks. The r/R between -1 to -0.6 and 0.6 to 1, that is, in the radial direction from the outer wall surface of the separator to the wall surface of vortex finder, the vorticity magnitude declines and then rises. The vorticity magnitude gradually decreases from the vortex finder wall to the geometric center of the cyclone. This is due to energy loss from vortex occurring near the wall. At z = 180 mm, the vorticity increases sharply near the oil return pipes, indicating that the breaking and energy loss of the vortex occur mainly near the oil return pipes. At z = 400 mm, the vorticity curves of the three cyclones are very close to each other with little deviation, indicating that The vortex in the upper part of the cyclone is less affected by the three different locations of the oil return pipe.

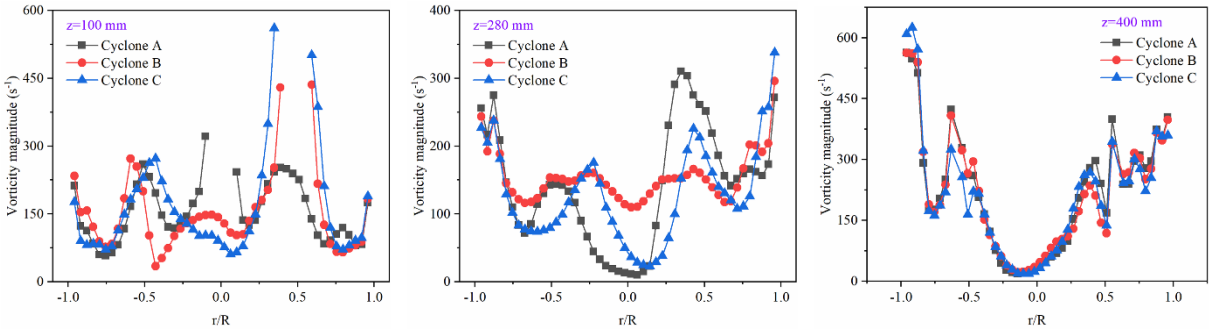

Figure. 7 The distribution curves of vorticity magnitude.

3.4. Tangential velocity field

The tangential velocity distribution in the cyclone is very important and can also reflect the characteristics of vortex. Figure. 8 gives the tangential velocity distribution curves in three cyclones. A Rankine vortex structure is visible in the tangential velocity distribution, that is, the internal is a quasi-forced vortex, whereas the external is a quasi-free vortex. The external quasi-free vortex is the main area for oil-gas separation [30]. At the three locations, it can be seen that the average tangential velocity in the external quasi-free vortex region is in the order of A > B > C. The greater the degree of vortex fragmentation caused by the return pipe, the more the tangential velocity decreases. As we all know, the centrifugal force is greatly affected by tangential velocity, the higher tangential velocity in the cyclone leads to the higher centrifugal force and is more advantageous the separation of oil droplets.

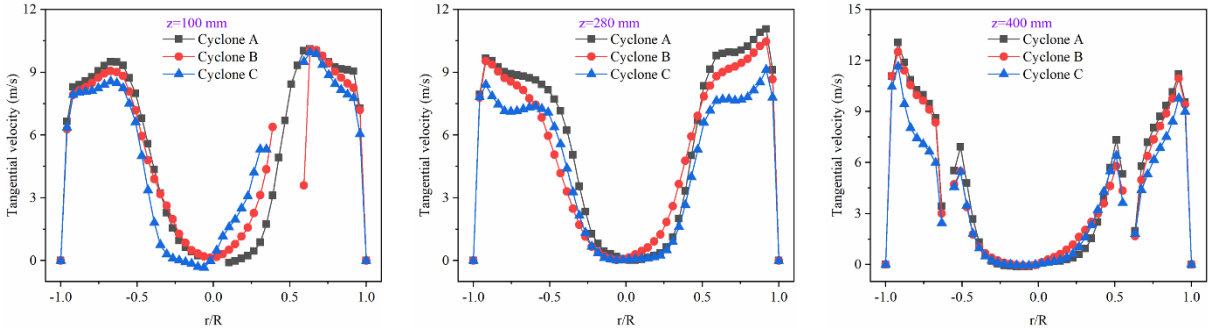

Figure. 8 The tangential velocity distribution of cyclones.

3.5. The separation efficiency

The separation efficiency is the most essential performance characteristic of a cyclone separator. Figure. 9 is the separation efficiency of the cyclone with three different oil return pipe locations. The order of separation efficiency for the same droplet diameter from highest to lowest is in agreement with the overall efficiency at the same inlet velocity. For oil droplets of 5 μm and above, the separation efficiency is essentially the same, having reached more than 97.5 %. For oil droplets below 5 μm, the maximum difference in separation efficiency between cyclone B and C is less than 1.25 %, which is relatively minor. The maximum difference in efficiency between cyclone B and A reaches 3.15 %, so the separation efficiency of cyclone A is higher than that of B and C for oil droplets below 5 μm. The oil return pipe location of cyclone A has better separation effect on smaller oil droplets. From the analysis of the vortex, this is because cyclone A has a less deformed and less fractured isovortex surface at the lower part of the cyclone and is closer to the geometric central axis. The flow field of cyclone A is more stable and more favorable for oil droplet separation. The analysis of vortex characteristics allows for a deeper understanding of how internal components of the oil-gas separator affect separation performance.

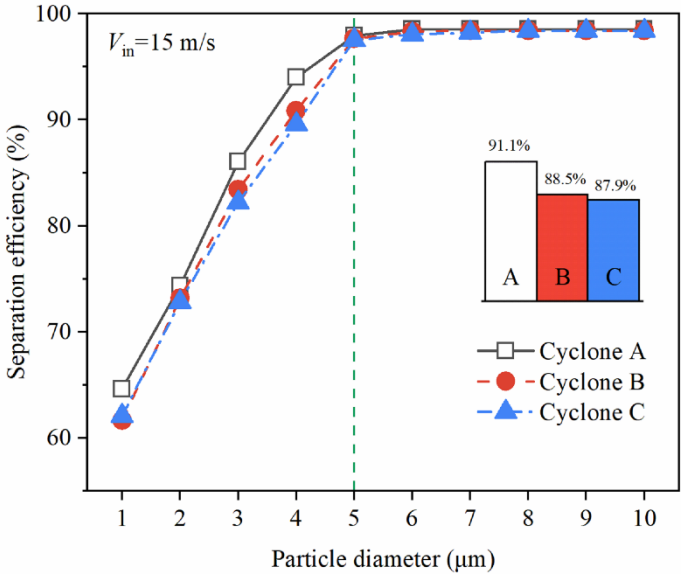

Figure. 9 The grade efficiency of three cyclones.

4. Conclusion

In this study, the effects of three different oil return pipe locations on the vortex characteristics of a cylindrical cyclone separator were investigated by CFD simulation based on the omega method, and the relationship with the separation performance was thoroughly analyzed. Several conclusions can be drawn as follows:

(1) The vortex deformation and breakup near the oil return pipe are evident, with the degree following the order of C > B > A, which is conducive to reducing pressure loss. Cyclone C, with the inclined return pipe, exhibits the lowest pressure drop. Compared to cyclones A and B, cyclone C has reduced pressure drop by 25.18 % and 15.85 %, respectively.

(2) At the tops of the three separators, the distribution patterns of vortex lines are similar, indicating that different return pipe positions have a relatively weak impact on the upper flow field of

the cyclone. However, at the bottom, cyclone A exhibits more symmetric and uniform vortex lines, with the vortex centers closer to the geometric center.

(3) The average tangential velocity in the external quasi-free vortex region follows the order A > B > C, attributed to varying degrees of vortex breakup, which corresponds to the overall separation efficiency order. For oil droplets of 5μm and larger, the separation efficiency is essentially the same, exceeding 97.5 %. Cyclone A exhibits the best separation effect for oil droplets smaller than 5μm.

Acknowledgment

The work was supported by the National Natural Science Foundation of China (Grant No. 50806055).

References

[1] Wu, W., *et al.*, Influence of evaporating rate on two-phase expansion in the piston expander with cyclone separator, *Thermal Science*, *24*. (2020), 3 Part B, pp. 2077-2088

[2] Wang, L., *et al.*, Experimental study on the separation performance of a novel oil–gas cyclone separator, *Powder Technology*, *415*. (2023), p. 118124

[3] Wu, H., *et al.*, Theoretical and experimental research on the working process of screw refrigeration compressor under superfeed condition, *International Journal of Refrigeration*, *30*. (2007), 8, pp. 1329-1335

[4] Wang, L., *et al.*, Performance Investigation and Optimization of the Primary Separation Part of the Oil-Gas Separator, *Industrial & Engineering Chemistry Research*. (2023),

[5] Gao, X., *et al.*, Numerical investigation of the effects of the central channel on the flow field in an oil–gas cyclone separator, *Computers & Fluids*, *92*. (2014), pp. 45-55

[6] Seon, G., *et al.*, Analysis of the impact of flow characteristics on the separation efficiency and pressure drop of a cyclone-type oil separator, *Journal of Mechanical Science and Technology*, *36*. (2022), 1, pp. 273-283

[7] Kim, H.S., *et al.*, Flow characteristics of refrigerant and oil mixture in an oil separator, *International Journal of Refrigeration*, *70*. (2016), pp. 206-218

[8] Balikci, A.,T. Koca, Experimental investigation on the effect of plunging pipe diameter change in cyclones to the performance of cyclones, *Thermal Science*. (2023), 00, pp. 116-116

[9] Alex, F.J., *et al.*, Bibliometric Network Analysis of Trends in Cyclone Separator Research: Research Gaps and Future Direction, *Sustainability*, *14*. (2022), 22, p. 14753

[10] Wakizono, Y., *et al.*, Effect of ring shape attached on upper outlet pipe on fine particle classification of gas-cyclone, *Separation and Purification Technology*, *141*. (2015), pp. 84-93

[11] Gong, A.,L.-Z. Wang, Numerical study of gas phase flow in cyclones with the repds, *Aerosol science and technology*, *38*. (2004), 5, pp. 506-512

[12] Liu, C., *et al.*, Experimental study and analysis on drag reduction mechanisms of reducing pressure drop stick in a cyclone separator, *Chemical Engineering & Technology: Industrial*

Chemistry - Plant Equipment - Process Engineering - Biotechnology, *29*. (2006), 4, pp. 495-503

[13] Brunnmair, E., *et al.*, Neuartiger gaszyklon mit differenzierter grob-und feinabtrennzone, *BHM Berg-und Hüttenmännische Monatshefte*, *12*. (2009), 154, pp. 610-613

[14] Pan, C., *et al.*, Research on the spiral guiding and the bash–mixing preventing of cyclone separating devises [J], *Chemical Industry and Engineering Progress*, *31*. (2012), 6, pp. 1215-1219

[15] Zhou, F., *et al.*, Experimental and CFD study on effects of spiral guide vanes on cyclone performance, *Advanced Powder Technology*, *29*. (2018), 12, pp. 3394-3403

[16] Chen, G., *et al.*, Experimental and CFD investigation on effects of internals on the flow pattern and performance of a divergent cyclone separator, *Journal of the Taiwan Institute of Chemical Engineers*, *115*. (2020), pp. 160-168

[17] Li, T., *et al.*, Numerical analysis of a novel cascading gas–liquid cyclone separator, *Chemical Engineering Science*, *270*. (2023), p. 118518

[18] Yao, Y., *et al.*, Double-eccentric design for the vortex finder of a cyclone separator, *Industrial & Engineering Chemistry Research*, *61*. (2022), 40, pp. 14927-14939

[19] Guo, M., *et al.*, Numerical investigation on the swirling vortical characteristics of a Stairmand cyclone separator with slotted vortex finder, *Powder Technology*. (2023), p. 118236

[20] Xu, J.,P. Hrnjak, Coalescing oil separator for compressors, *International Journal of Refrigeration*, *106*. (2019), pp. 41-53

[21] Le, D.K., *et al.*, A hybrid CFD–Deep Learning methodology to improve the accuracy of cut-off diameter prediction in coarse-grid simulations for cyclone separators, *Journal of Aerosol Science*, *170*. (2023), p. 106143

[22] Elhashimi, M.A., *et al.*, Unconventional desalination: The use of cyclone separators in HDH desalination to achieve zero liquid discharge, *Desalination*, *539*. (2022), p. 115932

[23] Huang, L., *et al.*, Numerical analysis of a novel gas-liquid pre-separation cyclone, *Separation and Purification Technology*, *194*. (2018), pp. 470-479

[24] Wang, B., *et al.*, Numerical study of gas–solid flow in a cyclone separator, *Applied Mathematical Modelling*, *30*. (2006), 11, pp. 1326-1342

[25] Chu, K., *et al.*, CFD–DEM simulation of the gas–solid flow in a cyclone separator, *Chemical Engineering Science*, *66*. (2011), 5, pp. 834-847

[26] Li, W., *et al.*, Effects of different cylinder roof structures on the vortex of cyclone separators, *Separation and Purification Technology*, *296*. (2022), p. 121370

[27] Liu, C., *et al.*, New omega vortex identification method, *Science China Physics, Mechanics & Astronomy*, *59*. (2016), pp. 1-9

[28] Dong, S., *et al.*, Experimental and numerical study on the performance and mechanism of a vortex-broken electrocyclone, *Chemical Engineering Journal*, *455*. (2023), p. 140758

[29] Zhang, Y., *et al.*, Heterogeneous condensation combined with inner vortex broken cyclone to achieve high collection efficiency of fine particles and low energy consumption, *Powder*

Technology, 382. (2021), pp. 420-430

[30] Wang, Q.-q., *et al.*, Design and performance study of a two-stage inline gas-liquid cyclone separator with large range of inlet gas volume fraction, *Journal of Petroleum Science and Engineering, 220*. (2023), p. 111218

Submitted: 05.02.2023.
Revised: 25.08.2023.
Accepted: 30.08.2025